AN OPTICAL STUDY OF BG GEMINORUM: AN ELLIPSOIDAL BINARY WITH AN UNSEEN PRIMARY STAR

PRISCILLA BENSON,[1] ALLYN DULLIGHAN,[2] ALCESTE BONANOS,[1] K. K. MCLEOD, AND [1] SCOTT J. KENYON[3]

ABSTRACT

We describe optical photometric and spectroscopic observations of the bright variable BG Geminorum. Optical photometry shows a pronounced ellipsoidal variation of the K0 I secondary, with amplitudes of ~ 0.5 mag at $VR_C I_C$ and a period of 91.645 days. A deep primary eclipse is visible for $\lambda \lesssim 4400$ Å; a shallower secondary eclipse is present at longer wavelengths. Eclipse timings and the radial velocity curve of the K0 secondary star indicate an interacting binary where a lobe-filling secondary, $M_2 \sim 0.5\ M_\odot$, transfers material into a extended disk around a massive primary, $M_1 \sim 4.5\ M_\odot$. The primary star is either an early B-type star or a black hole. If it did contain a black hole, BG Gem would be the longest period black hole binary known by a factor of 10, as well as the only eclipsing black hole binary system.

Key words: binaries: eclipsing — binaries: spectroscopic — stars: emission-line, Be — stars: evolution — stars: individual (BG Gem)

1. INTRODUCTION

BG Geminorum was discovered by Hoffmeister (1933) and Jensch (1938) as a possible RV Tauri star with an uncertain period of ~ 60 days. With a photographic magnitude of ~ 14, the star languished in the General Catalog of Variable Stars (Kholopov 1985) until 1992, when we began photometric observations to improve the period estimate and to verify the RV Tau classification. Early data revealed a repeatable ellipsoidal variation with a long period, instead of the more irregular variation expected from an RV Tau star. Additional photometry allowed us to refine the period and plan spectroscopic observations. Together with the photometry, high-quality spectra acquired around the orbit establish BG Gem as a rare eclipsing binary system with an unseen primary star and a lobe-filling K-supergiant secondary star.

This paper describes our data and analysis. We begin with a summary of the observations in § 2, continue with a detailed analysis in § 3, and conclude with the discussion in § 4.

2. OBSERVATIONS

Various student observers acquired optical photometry of BG Gem with standard $VR_C I_C$ filters and a Photometrics PM512 camera mounted on the Wellesley College 0.6 m Sawyer telescope. Observations beginning 23 July 1997 used a TK1024 back-illuminated CCD. We processed the data using standard tasks within NOAO IRAF.[4] Each image was bias-subtracted, dark-subtracted, and flat-fielded using twilight flats. We extracted photometry of BG Gem and several comparison stars using PHOT with a 3″ aperture and a 3″ sky annulus 17″ from the star. Wellesley is not

a photometric site; we thus derived photometry of BG Gem relative to comparisons verified to be nonvariable. The relative photometry has 1 σ probable errors of ± 0.011 mag at V, ± 0.014 mag at R_C, and ± 0.011 mag at I_C, based on repeat observations of comparison stars in the field of BG Gem. Table 1 lists the relative photometry of BG Gem and a comparison star as a function of time (the Heliocentric Julian Date, JD) and photometric phase ϕ defined below.

P. Berlind, M. Calkins, and several other observers acquired low-resolution optical spectra of BG Gem with FAST, a high-throughput slit spectrograph mounted at the Fred L. Whipple Observatory (FLWO) 1.5 m telescope on Mount Hopkins, Arizona (Fabricant et al. 1998). We used a 300 g mm^{-1} grating blazed at 4750 Å, a 3″ slit, and a thinned Loral 512×2688 CCD. These spectra cover 3800–7500 Å at a resolution of ~ 6 Å. We flux- and wavelength-calibrated the spectra in IRAF. After trimming the CCD frames at each end of the slit, we corrected for the bias level, flat-fielded each frame, applied an illumination correction, and derived a full wavelength solution from calibration lamps acquired immediately after each exposure. The wavelength solution for each frame has a probable error of ± 0.5–1.0 Å. We extracted object and sky spectra using the optimal extraction algorithm within APEXTRACT. The absolute flux calibration for each night relies on observations of 2–5 standard stars (Barnes & Hayes 1982) and has an uncertainty of $\pm 5\%$–10%. Nights with clouds or poor seeing have poor absolute calibrations ($\pm 20\%$ or worse) but good relative calibrations.

Figure 1 shows a typical spectrum of BG Gem. The spectrum resembles a late G or early K star, with a red continuum and strong absorption from the G band, Mg I, Na I, and the Ba I blend at $\lambda 6495$. Strong H I Balmer emission lines are also visible, with H10 and H11 present on some spectra. The Hα and Hβ lines are often double peaked. Some spectra show a weak blue continuum and weak He I emission at 5876 and 6678 Å. There is no evidence for absorption lines from a hot, early-type star.

To analyze the spectra, we measured continuum magnitudes and indices of strong absorption and emission lines using narrow passbands (O'Connell 1973; Worthey 1994). Table 2 lists the central wavelength λ and width $\delta\lambda$ for each.

[1] Wellesley College, Whitin Observatory, 106 Central St., Wellesley, MA 02181-8286.
[2] Dept. of Physics and Astronomy, Swarthmore College, 500 College Ave., Swarthmore, PA 19081.
[3] Harvard-Smithsonian Center for Astrophysics, 60 Garden St., Cambridge, MA 02138.
[4] IRAF is distributed by the National Optical Astronomy Observatories, which is operated by the Association of Universities for Research in Astronomy, Inc., under contract to the National Science Foundation.

TABLE 1

OPTICAL PHOTOMETRY

JD	Phase	δV(BG)	δV(com)	δR_C(BG)	δR_C(com)	δI_C(BG)	δI_C(com)
48694.5086	0.705	+0.187	1.154	+0.023	1.125	−0.161	1.122
48698.5333	0.749	+0.151	1.147	+0.059	1.115	−0.172	1.122
48984.5759	0.870	+0.354	1.133	+0.167	1.135	−0.037	1.118
48990.7176	0.937	+0.492	1.158	+0.274	1.154	+0.036	1.141
49006.5533	0.110	+0.373	1.165	+0.200	1.121	−0.012	1.111
49044.5032	0.524	+0.835	1.161	+0.635	1.123	+0.435	1.130
49084.5480	0.961	+0.566	1.145	+0.317	1.116	+0.070	1.147
49106.5242	0.201	+0.195	1.136	+0.008	1.142	−0.180	1.134
49368.7090	0.062	+0.477	1.169	+0.277	1.142	+0.081	1.123
49375.6981	0.138	+0.313	1.151	+0.110	1.132	−0.069	1.125
49382.7523	0.215	…	…	−0.007	1.185	−0.157	1.126
49390.6297	0.301	+0.193	1.157	+0.025	1.141	−0.132	1.112
49391.5136	0.311	+0.190	1.137	+0.002	1.143	−0.171	1.127
49398.5720	0.388	+0.373	1.160	+0.203	1.143	+0.027	1.119
49402.7024	0.433	+0.513	1.149	+0.371	1.111	+0.152	1.131
49406.6050	0.475	+0.784	1.156	+0.603	1.173	+0.411	1.125
49409.4841	0.507	+0.879	1.162	+0.637	1.143	+0.430	1.136
49410.6664	0.520	+0.899	1.146	+0.649	1.139	+0.484	1.119
49411.5224	0.529	+0.838	1.156	+0.625	1.139	+0.396	1.155
49412.5232	0.540	+0.810	1.154	+0.588	1.138	+0.348	1.143
49413.5668	0.551	+0.702	1.150	+0.462	1.122	+0.302	1.118
49416.5775	0.584	+0.533	1.168	+0.326	1.134	+0.116	1.118
49423.6071	0.661	+0.283	1.147	+0.110	1.133	−0.055	1.123
49435.6265	0.792	…	…	+0.034	1.164	−0.115	1.120
49438.5772	0.824	+0.271	1.138	+0.048	1.155	−0.107	1.118
49442.5804	0.868	+0.335	1.167	+0.166	1.150	+0.009	1.116
49443.6201	0.879	+0.377	1.156	+0.170	1.134	+0.035	1.103
49444.5683	0.890	+0.400	1.158	+0.213	1.147	+0.041	1.132
49447.5587	0.922	+0.438	1.151	+0.253	1.113	+0.047	1.132
49461.5167	0.075	+0.408	1.171	+0.230	1.136	+0.045	1.131
49744.6085	0.164	+0.229	1.155	+0.049	1.134	−0.099	1.114
49746.6087	0.185	+0.182	1.169	+0.028	1.143	−0.127	1.116
49747.6180	0.197	+0.171	1.176	−0.021	1.147	−0.164	1.120
49748.5698	0.207	+0.174	1.161	−0.003	1.143	−0.153	1.116
49751.6107	0.240	+0.076	1.166	−0.088	1.147	−0.202	1.102
49752.5963	0.251	+0.115	1.145	…	…	−0.197	1.114
49755.5755	0.283	+0.134	1.163	−0.021	1.135	−0.186	1.111
49757.5714	0.305	+0.165	1.158	+0.007	1.126	−0.151	1.110
49761.5820	0.349	+0.235	1.174	+0.061	1.144	−0.082	1.122
49762.5920	0.360	+0.251	1.165	+0.080	1.126	−0.056	1.112
49763.5168	0.370	+0.255	1.169	+0.089	1.143	−0.062	1.121
49766.5277	0.403	+0.381	1.150	+0.213	1.124	+0.040	1.125
49771.5679	0.458	+0.703	1.170	+0.504	1.159	+0.338	1.118
49780.6224	0.557	+0.621	1.170	+0.410	1.160	+0.246	1.111
49781.6495	0.568	+0.581	1.150	+0.347	1.136	+0.160	1.124
49804.5517	0.818	+0.256	1.159	+0.053	1.142	−0.112	1.125
49810.5121	0.883	+0.360	1.171	+0.144	1.154	−0.013	1.117
49815.5164	0.937	+0.455	1.169	+0.223	1.149	+0.056	1.109
49831.5523	0.112	+0.381	1.162	+0.158	1.144	+0.001	1.117
50114.6766	0.202	+0.141	1.155	−0.018	1.152	−0.162	1.119
50118.6449	0.245	+0.111	1.172	−0.045	1.154	−0.199	1.131
50120.6499	0.267	+0.133	1.157	−0.023	1.142	…	…
50131.5678	0.386	+0.310	1.162	+0.145	1.141	−0.022	1.120
50132.5850	0.397	+0.342	1.165	+0.186	1.140	+0.016	1.127
50139.6648	0.474	+0.702	1.172	+0.523	1.148	+0.353	1.126
50140.5501	0.484	+0.736	1.157	+0.548	1.140	+0.383	1.116
50143.5953	0.517	+0.777	1.171	+0.587	1.149	+0.403	1.137
50146.6049	0.550	+0.646	1.161	+0.456	1.140	+0.266	1.124
50147.5501	0.560	+0.602	1.174	+0.394	1.139	+0.207	1.121
50153.5759	0.626	+0.317	1.161	+0.136	1.139	−0.046	1.116
50160.5511	0.702	+0.128	1.179	−0.034	1.156	−0.198	1.132
50161.5227	0.713	+0.142	1.170	−0.025	1.157	−0.186	1.126
50462.6408	0.999	+0.633	1.166	+0.392	1.153	+0.185	1.121
50463.6463	0.009	+0.620	1.167	+0.398	1.142	+0.178	1.125
50472.6658	0.108	+0.369	1.155	+0.160	1.140	−0.015	1.109

TABLE 1—*Continued*

JD	Phase	$\delta V(BG)$	$\delta V(com)$	$\delta R_C(BG)$	$\delta R_C(com)$	$\delta I_C(BG)$	$\delta I_C(com)$
50489.5630	0.292	+0.137	1.147	−0.013	1.138	−0.175	1.121
50490.6027	0.304	+0.136	1.161	…	…	…	…
50504.5811	0.456	+0.679	1.167	+0.494	1.120	+0.288	1.162
50523.5677	0.663	+0.241	1.124	+0.107	1.101	−0.117	1.116
50782.8269	0.492	+0.792	1.158	+0.603	1.138	+0.431	1.122
50828.6566	0.992	+0.644	1.153	+0.398	1.134	+0.170	1.125
50836.5599	0.079	+0.374	1.159	+0.177	1.143	+0.015	1.132
50839.5264	0.111	+0.268	1.144	+0.140	1.118	−0.045	1.107
50840.5498	0.122	+0.329	1.164	+0.125	1.124	−0.069	1.122
50858.6164	0.319	+0.163	1.164	+0.022	1.154	−0.163	1.131
50860.6880	0.342	+0.224	1.158	+0.064	1.140	−0.085	1.099
50883.6207	0.592	+0.407	1.144	+0.218	1.131	+0.052	1.132
50897.5577	0.744	+0.156	1.163	−0.008	1.131	−0.165	1.124
50898.5383	0.755	…	…	−0.016	1.134	−0.168	1.119
50903.5061	0.809	+0.173	1.151	+0.005	1.149	−0.149	1.134
50914.5891	0.930	+0.432	1.161	+0.221	1.147	+0.036	1.148
50915.5573	0.941	+0.453	1.168	+0.247	1.145	+0.057	1.126
50931.5498	0.115	…	…	+0.077	1.175	−0.077	1.142
50932.5137	0.126	+0.251	1.168	+0.068	1.158	−0.095	1.122
51210.6585	0.161	+0.262	1.142	+0.059	1.137	−0.116	1.136
51219.5829	0.258	+0.145	1.159	−0.017	1.143	−0.179	1.121
51225.5590	0.323	+0.192	1.157	+0.024	1.147	−0.136	1.123
51226.6063	0.335	+0.213	1.166	+0.050	1.147	−0.097	1.121
51233.5798	0.411	+0.426	1.167	+0.265	1.133	+0.089	1.122
51240.5426	0.487	+0.844	1.151	+0.626	1.140	+0.444	1.107
51248.5614	0.574	+0.487	1.135	+0.245	1.145	+0.019	1.111
51255.5686	0.651	+0.381	1.140	+0.195	1.154	−0.028	1.128
51263.4974	0.737	+0.206	1.165	+0.001	1.144	−0.174	1.128
51269.5027	0.803	+0.250	1.150	+0.064	1.129	−0.139	1.125
51273.5037	0.846	+0.309	1.158	+0.113	1.148	−0.059	1.131
51277.6396	0.892	+0.309	1.192	+0.107	1.171	−0.033	1.133

The continuum magnitudes are normalized to the zero point of the V magnitude scale, $m_\lambda = -2.5 \log F_\lambda - 21.1$, where F_λ is the flux in the passband. The absorption and emission indices, derived using SBANDS within IRAF, are $I_\lambda = -2.5 \log (F_\lambda/\bar{F})$, where F_λ is the average flux in the passband λ and $\bar{F}$ is the continuum flux interpolated between the fluxes in the neighboring blue band centered at λ_b and the red band centered at λ_r. Table 3 lists the measured indices, along with emission-line equivalent widths, as a function of JD and ϕ. Table 4 lists continuum magnitudes measured on spectrophotometric nights.

We searched various databases for previous observations of BG Gem. BG Gem is not a known point source in any of the online *IRAS*, radio, or X-ray catalogs (e.g., *ASCA*, *ROSAT*). It lies close to several triggers in the CGRO/ BATSE 4B catalog (e.g., trigger 4157), but large positional offsets from the nominal trigger positions makes association with these events unlikely. The average of 100 days of data from the All-Sky Monitor (ASM) of the *Rossi X-ray Timing Explorer* is -0.1 ± 1.0 mCrab at 2–12 keV (R. Remillard 1999, private communication; 1 mCrab is 0.0755 counts s^{-1} with the ASM; see Levine et al. 1996), which corresponds roughly to $\sim 10^{-11}$ ergs cm^{-2} s^{-1} at 2–12 keV, assuming a
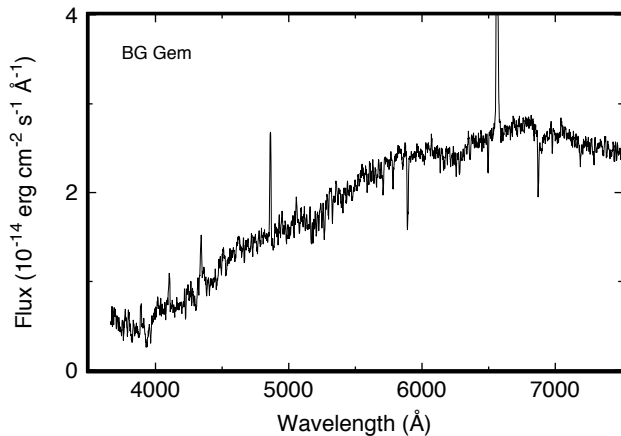

FIG. 1.—Optical spectrum of BG Gem. Strong H I emission lines and a faint blue continuum shortward of 4000 Å are produced by the hot primary. The red continuum and prominent Mg I and Na I absorption lines are from the K0 I secondary star.

TABLE 2
DEFINITIONS OF SPECTRAL INDICES

Feature	Name	λ	λ_b	λ_r	$\delta\lambda$
He I	I_{He}	6678	6600	6750	30
Hα	$I_{H\alpha}$	6563	6525	6600	30
Ba I	I_{Ba}	6495	6475	6525	25
Na I	I_{Na}	5893	5825	5965	30
Mg I	I_{Mg}	5175	5050	5300	30
Hβ	$I_{H\beta}$	4861	4825	4900	30
Fe I	I_{Fe}	4392	4364	4448	35
7025 cont	m_{7025}	7025	…	…	30
6370 cont	m_{6370}	6370	…	…	30
5550 cont	m_{5550}	5550	…	…	30
4400 cont	m_{4400}	4400	…	…	30
4050 cont	m_{4050}	4050	…	…	30

TABLE 3
ABSORPTION AND EMISSION-LINE INDICES

JD	Phase	$I_{Fe\,I}$	$I_{Mg\,I}$	$I_{Na\,I}$	$I_{Ba\,I}$	EW(Hβ)	EW(Hα)
51070.0128	0.626	0.083	0.144	0.176	0.045	-8.5	-27.7
51070.0150	0.626	0.103	0.150	0.182	0.041	-9.1	-28.3
51086.0142	0.801	0.107	0.154	0.179	0.040	-7.9	-25.8
51101.0046	0.964	0.130	0.179	0.177	0.052	-5.8	-20.1
51102.9545	0.985	0.148	0.205	0.177	0.047	-2.6	-16.4
51109.9734	0.062	0.115	0.158	0.174	0.040	-9.5	-27.4
51115.9804	0.128	0.092	0.151	0.174	0.045	-8.6	-28.1
51129.9315	0.280	0.107	0.141	0.149	0.035	-6.6	-23.8
51132.9985	0.313	0.124	0.143	0.164	0.037	-7.0	-25.8
51135.9320	0.345	0.110	0.147	0.155	0.038	-7.0	-26.4
51138.9114	0.378	0.115	0.151	0.154	0.041	-7.6	-27.9
51141.9962	0.411	0.112	0.151	0.169	0.047	-9.5	-29.9
51144.8588	0.443	0.104	0.186	0.184	0.040	-10.5	-35.5
51147.9806	0.477	0.111	0.170	0.197	0.042	-13.0	-40.7
51157.7598	0.583	0.097	0.158	0.177	0.049	-10.7	-32.0
51160.8444	0.617	0.106	0.144	0.160	0.042	-9.2	-29.1
51163.9600	0.651	0.096	0.139	0.156	0.029	-8.7	-28.2
51166.8621	0.683	0.102	0.154	0.159	0.048	-7.8	-27.0
51169.8996	0.716	0.103	0.150	0.160	0.045	-7.0	-25.2
51172.8716	0.748	0.109	0.151	0.163	0.047	-7.6	-26.0
51175.9043	0.781	0.092	0.143	0.154	0.043	-8.3	-27.9
51187.7566	0.911	0.094	0.164	0.157	0.048	-10.7	-29.4
51188.7424	0.922	0.121	0.161	0.165	0.044	-9.4	-27.9
51191.7695	0.955	0.140	0.176	0.160	0.051	-6.4	-21.1
51194.8215	0.988	0.135	0.201	0.183	0.060	-2.0	-15.3
51196.7938	0.009	0.143	0.187	0.187	0.049	-2.9	-15.9
51198.7117	0.030	0.129	0.176	0.174	0.052	-5.1	-18.9
51201.7889	0.064	0.110	0.160	0.151	0.046	-9.8	-27.6
51216.6831	0.226	0.108	0.129	0.148	0.049	-7.3	-24.6
51218.6966	0.248	0.108	0.125	0.153	0.046	-6.9	-24.3
51223.5895	0.302	0.100	0.141	0.157	0.043	-7.1	-25.8
51224.6268	0.313	0.106	0.129	0.151	0.042	-7.0	-25.7
51226.7300	0.336	0.105	0.122	0.145	0.035	-6.8	-29.7
51228.6119	0.357	0.083	0.144	0.127	0.043	-7.2	-28.1
51230.7042	0.379	0.114	0.130	0.155	0.041	-8.3	-29.1
51232.7299	0.402	0.101	0.131	0.154	0.048	-8.8	-30.6
51247.7040	0.565	0.100	0.160	0.170	0.044	-12.8	-36.0
51249.5973	0.586	0.100	0.150	0.160	0.043	-11.0	-33.2
51257.6133	0.673	0.105	0.134	0.156	0.046	-8.6	-27.5
51259.6068	0.695	0.102	0.153	0.159	0.043	-8.0	-27.2
51278.6080	0.902	0.122	0.143	0.146	0.051	-9.1	-28.2
51280.6209	0.924	0.116	0.151	0.163	0.052	-8.7	-25.7
51284.6181	0.968	0.139	0.169	0.168	0.040	-3.3	-18.1
51287.6168	0.000	0.143	0.198	0.176	0.055	-1.7	-14.0
51289.6136	0.022	0.126	0.188	0.187	0.049	-4.1	-17.6
51291.6213	0.044	0.122	0.173	0.173	0.049	-8.3	-22.8

spectrum similar to that of other X-ray binaries; see Sobczak et al. 1999b). BG Gem is a 2MASS point source, 0603308 + 274150 in the 1999 Spring Release Point Source Catalog, as summarized below.

3. ANALYSIS

3.1. *The Light Curves*

Figure 2 shows light curves for BG Gem. The data have been folded on the best period derived from Fourier analysis and periodograms. The primary minimum has the ephemeris

$$\mathrm{Min} = \mathrm{JD}\ 2449179.7437 \pm 1.037 + (91.645 \pm 0.315) \times E\ .$$

$$(1)$$

We define $\phi = 0.0$ at primary minima. The curves at 4050 and 4400 Å are derived from FAST spectra. The zero points for the V and R data are set from FAST light curves at 5550 and 6500 Å using offsets derived from the Jacoby, Hunter, & Christian (1984) spectral atlas and published broadband magnitudes, $V = m_{5550} + 0.16$ and $R_C = m_{6475} - 0.48$. The zero point for the I_C light curve assumes that the secondary is a normal K0 I star reddened by $A_V \approx 1.65$ mag (see below), with an intrinsic $R_C - I_C = 0.52$ (Bessell 1990).

The light curves show several clear features. Ellipsoidal variations of the secondary star are prominent at $VR_C I_C$. The large amplitudes of ~ 0.5 mag indicate that the secondary probably fills its Roche lobe and that the orbital inclination is close to 90°. The deep primary minimum at short wavelengths shows that the primary star is much hotter than the secondary. The eclipse of the primary is long and

TABLE 4

CONTINUUM MAGNITUDES

JD	Phase	m_{4050}	m_{4400}	m_{5550}	m_{6370}	m_{7025}
51101.0046	0.964	15.19	14.40	13.33	13.15	13.07
51102.9545	0.985	15.34	14.59	13.47	13.35	13.20
51109.9734	0.062	14.40	14.05	13.05	12.87	12.82
51115.9804	0.128	14.35	14.00	13.06	12.89	12.80
51135.9320	0.345	14.31	13.99	13.06	12.89	12.87
51141.9962	0.411	14.29	14.06	13.18	13.05	13.07
51157.7598	0.583	14.57	14.17	13.13	12.94	12.90
51160.8444	0.617	14.43	14.07	13.09	12.94	12.93
51172.8716	0.748	14.10	13.75	12.83	12.69	12.65
51175.9043	0.781	14.21	13.86	12.91	12.76	12.74
51188.7424	0.922	14.44	14.05	13.15	13.08	13.07
51191.7695	0.955	15.02	14.55	13.45	13.26	13.20
51196.7938	0.009	15.33	14.65	13.48	13.29	13.13
51216.6831	0.226	14.32	13.91	13.07	12.91	12.77
51218.6966	0.248	14.23	13.80	13.06	12.92	12.84
51223.5895	0.302	14.31	13.90	13.04	12.90	12.85
51230.7042	0.379	14.22	13.92	12.97	12.84	12.81
51247.7040	0.565	14.70	14.32	13.33	13.15	13.15
51259.6068	0.695	14.26	13.86	12.91	12.81	12.72
51278.6080	0.902	14.45	14.07	13.16	13.06	13.01
51280.6209	0.924	14.41	14.04	13.10	13.00	13.01
51287.6168	0.000	15.36	14.65	13.47	13.34	13.22
51289.6136	0.922	14.44	14.05	13.05	12.98	12.95
51291.6213	0.944	14.77	14.28	13.24	13.06	13.01

flat bottomed, which implies that the primary is extended. This extended primary is probably responsible for the eclipse of the secondary star visible in the V, R_C, and I_C filters as a deep secondary minimum at $\phi = 0.5$.

The absorption line indices shown in Figure 3 provide additional support for a hot, extended, primary star in BG Gem. Because of a decrease in the continuum flux, all of the lines are strongest during the eclipse of the primary. The blue lines strengthen much more than the red lines, indicating that the primary has a blue continuum. The eclipse of the primary covers a significant fraction, $\sim 10\%$, of the orbital period.

We can measure the spectral type of the secondary star by examining the absorption lines at $\phi = 0.0$, when the primary is in eclipse. Based on a comparison of the spectral indices with indices derived from the Jacoby et al. (1984) and Worthey (1994) spectral atlases, all of the absorption lines imply a late G or early K spectral type. Our best estimate is K0 I, with an uncertainty of 1–2 subclasses. The supergiant classification is required for the combination of strong Mg I, Na I, and Fe I absorption features. This result agrees with the low gravity implied for a lobe-filling secondary.

The Balmer emission-line equivalent widths also vary with phase (Fig. 4). The Hα and Hβ lines are eclipsed at primary minimum. The eclipses are long and never reach totality. Both lines strengthen relative to the continuum during secondary eclipses, because the flux from the K0 I secondary weakens considerably. Similar variations may be visible in He I $\lambda 6678$, but the line is weak, with a typical
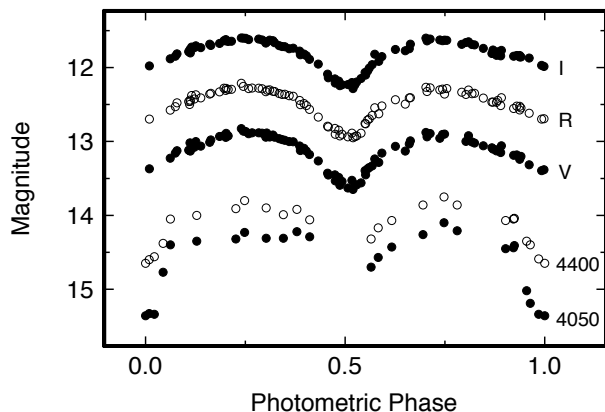

FIG. 2.—Optical light curves of BG Gem. Narrowband continuum magnitudes at 4050 and 4400 Å are from FAST spectra. Broadband magnitudes are from Wellesley CCD data scaled as described in the text. All light curves show ellipsoidal variations of the lobe-filling secondary and an eclipse of the hotter primary at phase 0.
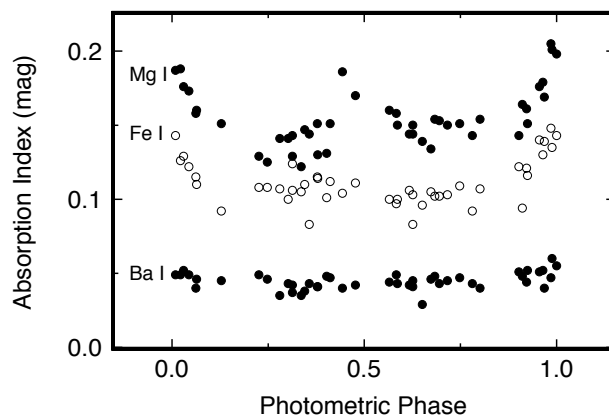

FIG. 3.—Variation of absorption line indices. The Ba I index at 6495 Å is nearly constant with phase. The Mg I and Fe I indices strengthen during primary eclipse. Blue absorption lines—e.g., Fe I λ 4400—strengthen relatively more than red absorption lines—e.g., Mg I λ 5200.
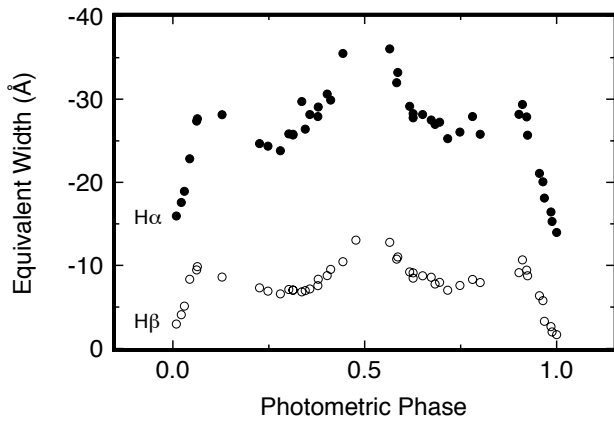
FIG. 4.—Variation of emission-line equivalent widths. The H I emission is eclipsed by the secondary at $\phi = 0$. The emission flux is roughly constant outside eclipse: the equivalent widths rise at $\phi = 0.5$, because the K0 continuum declines.

TABLE 5
RADIAL VELOCITIES

JD	Phase	$v_{\rm abs}$	$v_{\rm H\beta}$
2451070.0150	0.626	-19.0	41.8
2451086.0142	0.801	-36.9	41.2
2451101.0046	0.964	5.4	212.0
2451102.9545	0.985	-11.1	171.5
2451109.9734	0.062	56.9	49.3
2451115.9804	0.128	77.4	41.6
2451129.9315	0.280	98.5	56.7
2451132.9985	0.313	80.0	21.9
2451135.9320	0.345	82.1	24.2
2451138.9114	0.378	77.1	17.5
2451141.9962	0.411	80.2	32.1
2451144.8588	0.443	56.8	5.4
2451147.9806	0.477	24.5	32.7
2451157.7598	0.583	-23.2	18.0
2451160.8444	0.617	-29.6	48.2
2451163.9600	0.651	-30.6	33.9
2451166.8621	0.683	-48.6	35.2
2451169.8996	0.716	-31.2	55.1
2451172.8716	0.748	-36.6	57.3
2451175.9043	0.781	-35.0	25.7
2451187.7566	0.911	-5.2	61.9
2451188.7424	0.922	7.3	73.0
2451191.7695	0.955	12.7	207.9
2451194.8215	0.988	31.0	153.7
2451196.7938	0.009	42.6	-46.3
2451198.7117	0.030	50.2	-99.2
2451201.7889	0.064	87.1	23.8
2451216.6831	0.226	129.0	36.0
2451218.6966	0.248	118.0	66.0
2451223.5895	0.302	95.3	28.7
2451224.6268	0.313	125.0	31.7
2451226.7300	0.336	104.3	63.1
2451228.6119	0.357	41.8	27.6
2451230.7042	0.379	68.4	38.7
2451232.7299	0.402	43.8	16.8
2451247.7040	0.565	-10.3	4.5
2451249.5973	0.586	-21.4	16.0
2451257.6133	0.673	-54.3	12.0
2451259.6068	0.695	-40.9	43.0
2451278.6080	0.902	-3.2	74.9
2451280.6209	0.924	10.6	125.5
2451284.6181	0.968	18.3	178.2
2451287.6168	0.000	15.3	12.8
2451289.6136	0.022	33.4	-71.5
2451291.6213	0.044	55.2	-46.5

equivalent width of 0.5 Å or less. Other He I lines are too difficult to measure accurately: $\lambda 5876$ is blended with Na I, and $\lambda 7065$ is very weak.

The light curves constrain the sizes of the H II emission region and the primary and secondary stars. For an edge-on system with a circular orbit, the eclipse duration yields the sum of the radii of the two components; the duration of totality establishes the difference of the two radii. In BG Gem, the length of the eclipses at 4400 and 4050 Å results in $R_1 + R_2 \approx 0.37A$, where A is the orbital semimajor axis, R_1 is the radius of the primary star, and R_2 is the radius of the K0 I secondary star. From the length of totality, $R_2 - R_1 \approx 0.12A$. These two constraints set $R_1 \approx 0.12A$ and $R_2 \approx 0.25A$. The apparent length of totality at $\phi = 0.5$ in the R_C and I_C filters suggests a somewhat larger radius for the primary at long wavelengths. The length of the Hα eclipse implies $R_{\rm H\alpha} + R_2 \approx 0.55A$, which results in $R_{\rm H\alpha} \approx 0.3A$. The lack of a total eclipse for Hα confirms that the H II region is larger than the K0 I secondary.

To derive absolute constraints on the binary components, we need an independent measure of A. We now consider radial velocity data to establish the orbital parameters of BG Gem.

3.2. Radial Velocities

We derived radial velocities from the strong absorption and emission lines on FAST spectra. For absorption line velocities, we cross-correlated the FAST spectra against the best-exposed spectrum, where the velocity is set by cross-correlation against standard stars with known velocities (see Tonry & Davis 1979; Kurtz & Mink 1998). To avoid contamination from the hot primary, we restricted the cross-correlation to $\lambda\lambda 5000$–6800. We measured emission-line velocities from cross-correlations with an emission-line template, as described by Kurtz & Mink (1998). We adopted the velocity of Hβ as the emission-line velocity, because Hα may be blended with [N II] emission on our low-resolution spectra. We estimate errors of ± 15 km s^{-1} for absorption lines and ± 20 km s^{-1} for emission lines. Table 5 lists the measured velocities as a function of JD and ϕ.

Figure 5 shows the absorption line radial velocities as a function of photometric phase. We analyzed these obser-

vations using Monet's (1979) Fourier transform algorithm (see also Kenyon & Garcia 1986). The best spectroscopic period, $P_{\rm spec} = 90.18 \pm 5.28$, agrees with the photometric period. A circular orbit with $P = P_{\rm phot}$ from equation (1) fits the orbit well. This solution has an orbital semiamplitude, $K_{\rm K0} = 74.6 \pm 4.5$ km s^{-1}, and a fractional semimajor axis, $A_{\rm K0} \sin i = 0.63 \pm 0.04$ AU. Spectroscopic conjunctions occur 1.234 days prior to photometric minima,

$$\text{Conj} = \text{JD } 2451057.2325 \pm 0.957 + 91.645 \times \text{E} . \quad (2)$$

This phase difference has a significance of only 1.3 σ. The mass function is $M_1^3 \sin^3 i = (3.97 \pm 0.09) \, M_\odot (M_1 + M_{\rm K0})^2$. If we adopt $\sin i = 1$, this result becomes $M_1 \approx 4 \, M_\odot (1 + q)^2$, where $q \equiv M_{\rm K0}/M_1$ is the mass ratio.

Solutions with eccentric orbits do not improve the fit to the data. Iterations in Fourier and configuration space yield $e = 0.096 \pm 0.065$. The Lucy & Sweeney (1971) test con-
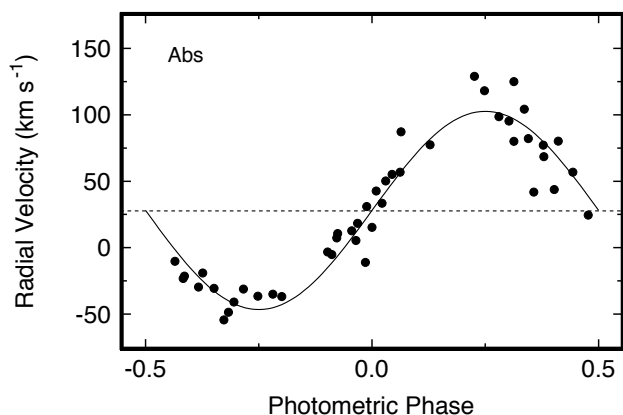
FIG. 5.—Absorption line radial velocity curve. The solid line is the best-fitting circular orbit to the measured velocities (*filled circles*). The dashed line indicates the systemic velocity. Note that we have centered this plot on $\phi = 0.0$ for clarity.

firms that the nonzero e has only 1.5 σ significance. We thus prefer the circular solution with the parameters quoted above. These results place a lower limit on the mass of the primary, $M_1 \gtrsim 4\ M_\odot$, if the K0 I secondary has negligible mass and $\sin i = 1$.

The emission-line velocities and double-peaked profiles indicate that the emission lines form in a circumstellar disk surrounding the primary star (Fig. 6). The Hβ line has a nearly constant velocity outside primary eclipse, with a mean velocity of $+33.8 \pm 16.3$ km s^{-1}. This velocity is identical to the systemic velocity $\gamma = 28.0 \pm 3.2$ km s^{-1}. The line velocity increases as the eclipse of the blue continuum begins. The velocity reaches $\gamma + 125$ km s^{-1} at $\phi = -0.05$ to -0.04, decreases to the systemic velocity at $\phi = 0.00$, falls to $\gamma - 125$ km s^{-1} at $\phi = 0.04$ to 0.05, and returns to the systemic velocity as the eclipse of the blue continuum ends. This classical disturbance—the Rossiter effect—is consistent with the eclipse of a rapidly rotating disk. The blue-shifted half of the disk is eclipsed first during ingress and is revealed first during egress. Both Hα and Hβ decrease in FWHM during eclipse, supporting this interpretation. If we associate the apparent rotational velocity of ~ 125–150 km s^{-1} with disk rotation, the radius of the disk is $R_{H\alpha} \approx$ 35–50 $R_\odot (M_1/4\ M_\odot)$. Together with our limit on
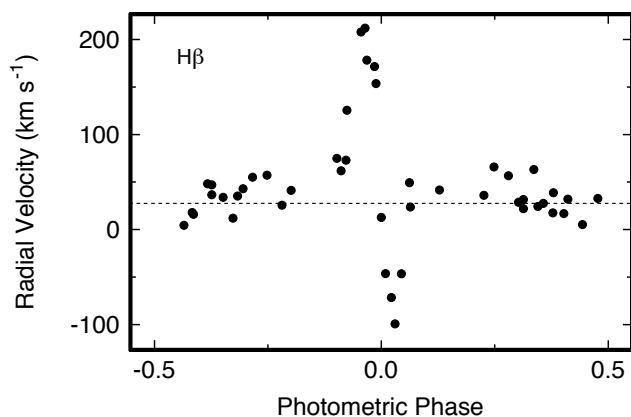
$R_{H\alpha}$ from the eclipse duration, this result leads to a rough estimate for the mass ratio, $q \sim 0.1$, and the semimajor axis, $A \approx 150\ R_\odot$.

The small mass ratio supports our conclusion that the K0 supergiant fills its Roche lobe. The effective radius of the Roche lobe for $q = 0.1 \pm 0.05$ is $R_L \approx 0.25^{+0.06}_{-0.04} A$, indistinguishable from our estimate for the radius of the secondary, $R_L \approx 0.25A$. The effective radius of the Roche lobe for the primary star is $R_L \approx 0.71^{+0.06}_{-0.07} A \approx 105 \pm 10\ R_\odot$. The radius of the H$\alpha$ emission region is thus roughly half of the tidal radius. The radius of the primary at blue wavelengths is only $\sim 20\%$ of the tidal radius, but is large compared with the radius of a normal main sequence star.

These results suggest a simple dynamical model for BG Gem. The system consists of a lobe-filling K0 supergiant that transfers material into a large luminous accretion disk surrounding a primary star with $M_1 \sim 4$–5 $M_\odot$. The disk must have a blue continuous spectrum to explain the deep primary eclipses at $\lesssim 4500$ Å. This disk is also responsible for the secondary eclipses at longer wavelengths.

To refine this model, we now consider the light curve and spectra in more detail. We begin with an analysis of the light curve using the Wilson-Devinney (1971) code. Improved constraints on the orbital parameters and on the physical characteristics of the binary components lead to better limits on the nature of the accretion disk. We then use the reddening derived from the Balmer lines and the optical continuum to set the distance to the system.

3.3. Detailed Light-Curve Analysis

Wilson & Devinney (1971) developed a modern light-curve synthesis program to derive physical characteristics of binary stars from multicolor light curves. Wilson (1990, 1994, and references therein) describes recent improvements to the code, which is now available by anonymous ftp. The code consists of two programs: LC, used to compute model light curves or radial velocity curves as a function of various input parameters; and DC, which can be iterated to derive the best set of binary parameters from a least-squares fit of the model to actual observations. The analysis of §§ 3.1 and 3.2 demonstrates that the primary component of BG Gem is an extended disk surrounding a massive star. We view the system at close to $90°$. Few light-curve synthesis programs include radiation from a disk; none reliably compute fluxes for an edge-on disk. Therefore, for this study, we used LC to derive reliable ranges for binary parameters that produce light curves similar to those in Figures 2–4 but omitted the iteration of these parameters with DC.

Figure 7 shows light curves from Figure 2 along with model light curves. To determine the best-fit binary system (*dashed curves*), we varied several parameters to derive a "best" approximation to the observations, (1) the mass ratio, q; (2) the inclination, i; and (3) the brightness of the primary star relative to a lobe-filling secondary with an effective temperature, 4500 K, appropriate for a K0 supergiant star. The mass ratio and inclination set the amplitude of the ellipsoidal variations; the ellipsoidal amplitude grows with $\sin i$ and inversely with q. The relative brightness of the primary sets the depth of the primary eclipse and is also constrained by the variation of absorption line indices with wavelength.

The dashed light-curve models in Figure 7 have several successes and failures. The models match the depth of primary eclipse at each wavelength and the overall ampli-

FIG. 6.—Emission-line radial velocity data for Hβ. The dashed line indicates the systemic velocity. Note that we have centered this plot on $\phi = 0.0$ for clarity.
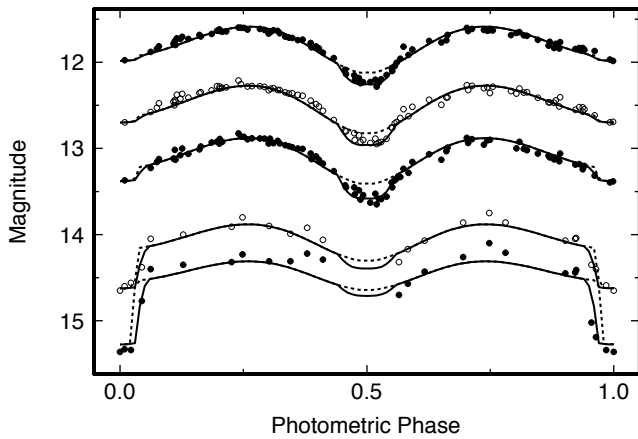
FIG. 7.—Comparison of binary models with observations. Observations are as in Fig. 2. Model light curves, dashed lines for a binary with a small B-type primary star and a lobe-filling K0 star with $q = 0.1$ and $i = 90°$, and solid lines for a disk-shaped primary. At $\phi = 0.25$, the B-type primary emits 40% at 4050 Å, 25% at 4400 Å, 9% at 5500 Å, 5% at 6500 Å, and 3% at 8000 Å. Compared with the stellar primary (*dashed lines*) a disk with a rectangular cross section (*solid lines*)—described in the text—produces more rounded eclipses at $\phi = 0.0$ and deeper eclipses at $\phi = 0.5$.

tude and shape of the light curves at $\phi \approx 0.05–0.40$ and $\phi \approx 0.60–0.95$. The length of the model eclipse at $\phi = 0$ is too short, because the model primary is a star instead of a disk. The secondary minimum at $\phi = 0.5$ is too shallow, because the small primary star cannot eclipse very much of the lobe-filling K0 I secondary. The primary star must be hot and small to match the depths of primary eclipse at 4000–9000 Å.

To make a more realistic light-curve synthesis, we considered a crude disk model for the primary star (*solid curves* in Fig. 7). We assumed a disk with a rectangular cross section, as viewed in the orbital plane. This disk has height H_d above the orbital plane and radius R_d in the orbital plane. We assumed $R_d = \beta(\phi)R_L$ and $H_d = 0.05–0.1R_d$, where R_L is the effective radius of the Roche lobe of the primary. We then took the output of LC—the fluxes of the primary and secondary as a function of ϕ—and constructed new model light curves. We computed (1) the fraction of the disk eclipsed by the K0 secondary star at $\phi = 0.0 \pm 0.1$, and (2) the fraction of the K0 secondary eclipsed by the disk at $\phi = 0.5 \pm 0.1$. We accurately accounted for Roche geometry and assumed that both light sources are completely opaque and uniformly illuminated. This approach ignored limb and gravity darkening of the secondary but should yield light curves closer to those actually observed.

The simple disk-shaped primary can explain the depths and shape of both primary and secondary eclipses, as indicated by the solid lines in Figure 7. Models with $H_d = 0.07R_d$, $\beta(\phi = 0.0) \sim 0.2$, and $\beta(\phi = 0.5) \sim 0.8–0.9$ yield the "best" fit to the data. Less extended disks do not eclipse enough of the secondary at $\phi = 0.5$. More extended disks occult too much of the secondary. The large variation in disk radius with orbital phase suggests that the opaque, outer part of the disk is much cooler than the inner part of the disk. Our model is too simple to constrain either the size of the disk as a function of wavelength or the brightness temperature distribution within the disk, as in Vrielmann, Horne, & Hessman (1999), for example. We plan more detailed analyses in future studies.

The models shown in Figure 7 assume $i = 90°$, $q = 0.1$, and a primary star with an effective temperature of 10,000 K. Primary stars with different effective temperatures do not change the model light curves as long as the ratio of the luminosity of the primary star to the luminosity of the secondary star at each wavelength remains fixed. These ratios are set by the eclipse depth and cannot vary by much more than 10%. For fixed inclination, smaller mass ratios produce shallower secondary mimina. The disk radius also shrinks as q increases, which leads to a smaller "disk eclipse" at secondary minimum. We estimate $q = 0.1 \pm 0.05$ for $\sin i = 1$. Any geometry with $i \lesssim 80°$ does not produce a primary eclipse and is thus ruled out by the data. Improved constraints on these values using our data requires a WD-type code that includes a reliable model for an edge-on accretion disk.

3.4. The Nature of the Primary

To derive better limits on the nature of the primary star, we need good estimates for the reddening and distance in addition to the parameters derived above. With $l = 183°$ and $b = 2°.8$, BG Gem lies close to the Galactic plane in the direction of the Galactic anticenter. Previous extinction surveys suggest modest visual extinctions, $A_V \sim 1–2$ mag, for distances of 1–5 kpc (e.g., Neckel & Klare 1980; Hakkila et al. 1997). Adopting $A_V = 1.5 \pm 0.5$ mag yields $V_0 = 11.5 \pm 0.5$ for the system at maximum and $d = 2.5 \pm 0.5$ kpc for a K0 I star with $M_{bol} = -1.9$ from the LC program and a bolometric correction of 1.5 mag.

We can place better limits on the extinction from near-IR photometry and the emission-line data. A K0 supergiant should have $V - J = 1.5–1.6$ and $V - K = 2.1–2.3$. Data from 2MASS—$J = 10.32 \pm 0.03$, $H = 9.61 \pm 0.03$, and $K = 9.34 \pm 0.03$—and $V = 13.0$ at maximum imply $A_V = 1.65 \pm 0.25$ for a normal extinction law (e.g., Rieke & Lebofsky 1985; Bessell & Brett 1988). The mean intensity ratio for Hα and Hβ is $I(H\alpha)/I(H\beta) = 5.81 \pm 1.01$; this ratio suggests $A_V = 1.6 \pm 0.5$ for a standard extinction law (Mathis 1990). We thus favor $A_V = 1.65 \pm 0.25$ for the extinction and $d = 2.25 \pm 0.25$ kpc. This combination agrees with the distance-dependent extinction measurements summarized in Hakkila et al. (1997).

Figure 8 shows the observed spectral energy distribution for BG Gem. Filled points indicate observations dereddened by $A_V = 1.65$. The K0 supergiant produces most of the optical and near-infrared radiation, as indicated by the solid and dot-dashed curves. The primary source contributes a modest fraction of the V light. Its fraction of the total light grows substantially toward shorter wavelengths, as shown by the dashed curve. The slope of the hot continuum, $\alpha = (d \log F_\lambda/d \log \lambda) = -2.5 \pm 0.75$, is best fitted by the spectrum of an accretion disk but is marginally consistent with the spectrum of an early type star. The measured extent of the primary, $R_1 \approx 18 \pm 2 R_\odot$, is much larger than a normal early-type main sequence star. The predicted V magnitude of a spherical star with $T \geq 10^4$ K and $R_1 \approx 18 R_\odot$ is roughly 2–3 mag *brighter* than the K0 secondary. Our observed limit on the V brightness of the primary, $\sim 10\%$ of the K0 secondary, demonstrates that the primary is not a star. However, a flattened disk with $H_d/R \sim 0.05–0.10$ satisfies the limits on R_1 and the total brightness derived from the light curves.

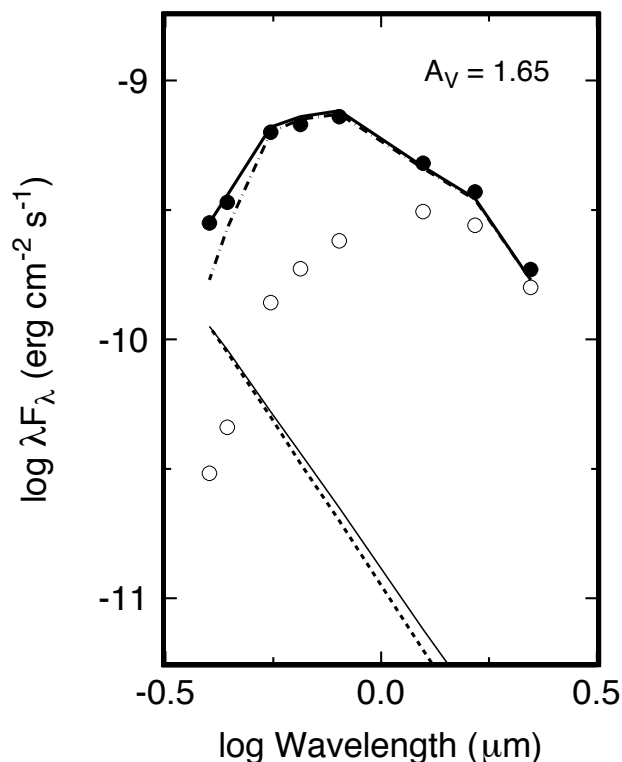Constructing a "best" model for the disk in BG Gem requires ultraviolet or X-ray data to provide better con-

FIG. 8.—Spectral energy distribution of BG Gem. The open circles indicate observed fluxes; filled circles indicate dereddened fluxes. The dot-dashed line plots the spectrum of a K0 I star normalized to emit 60% of the flux at 4050 Å. The dashed line plots the spectrum of the primary, log $\lambda F_\lambda \propto \lambda^{-2.5}$, normalized to emit 40% of the 4050 Å flux. The heavy solid line shows the combined flux of the K0 supergiant and the primary. The light solid line indicates the spectrum of the disk model described in the text.

straints on the spectrum and on the radius of the primary star. In this paper, we simply develop a model consistent with the observed spectrum and masses without considering whether it is "best" or unique. We first examine the case where the disk surrounds a hot primary star with parameters defined in § 3.3. The primary star either has a low luminosity compared with the disk or is occulted by the disk. Otherwise, our model cannot account for the primary eclipse as outlined above. Requiring a self-luminous disk to produce all of the optical flux yields a large accretion rate, $\dot{M} \gtrsim 10^{-5}\ M_\odot\ \mathrm{yr}^{-1}$, which is ruled out by the weak H I emission and the lack of high-ionization lines, such as He II $\lambda 4686$, on the optical spectrum (see Kenyon & Webbink 1984). A "reprocessing" disk—which absorbs and reradiates light from the primary—can have a spectrum similar to a viscous accretion disk, because the temperature distributions are similar (Kenyon & Hartmann 1987). Tests of several purely reprocessing disk models surrounding B-type stars indicate, however, that the half-light radius of the disk is $\sim 10\ R_\odot$, instead of the $\sim 20\ R_\odot$ derived from the optical eclipses. We thus consider models where accretion and reprocessing contribute comparable amounts to the observed spectrum.

The light solid line in Figure 8 plots the spectrum from an accretion disk that satisfies several observational constraints. The disk surrounds a B3 main-sequence star. A large inclination, $i \geq 85°$, allows the central star to hide behind the outer parts of the disk. The disk may also shield

the K0 star from the radiation field of the B star. An accretion rate of a few $\times 10^{-6}\ M_\odot\ \mathrm{yr}^{-1}$ provides roughly half of the observed continuum radiation. The model predicts a disk temperature $\sim 10^4$ K at a disk radius $\sim 20\ R_\odot$ and a temperature ~ 3000 K at ~ 80–$90\ R_\odot$. These results are consistent with eclipse data that require a small hot primary at short wavelengths and a larger, cooler primary at long wavelengths (§ 3.3). Cool material in the outer disk may also produce the extra Mg I absorption implied by the apparent rise in the Mg I index at secondary minimum (Fig. 5). The uncertainties in this model are modest if we require the primary to lie on the main sequence. Stars much cooler than $\sim 15,000$ K (B6 V) produce disks that are too cold to match the optical spectrum. Stars much hotter than $\sim 30,000$ K (B0) should produce substantial He I emission (from ionization of the disk) that is not observed.

This model has one main failure. It is difficult for a B3 star to produce enough photons to ionize H to the observed level. We estimate an extinction-corrected Hβ luminosity of $0.2\ L_\odot$, which requires $\sim 4 \times 10^{45}$ H-ionizing photons s^{-1} if the B star ionizes material in the disk. This limit is 1–2 orders of magnitude larger than is expected from a B3 V star. A boundary layer at the inner edge of the disk probably also produces too few ionizing photons, unless we have underestimated the accretion rate (see, for example, Kenyon et al. 1991). Olson (1991) considered Hα line formation within the disks of several Algol systems and produced line profiles similar to those observed. It may be possible to account for the line flux in a similar way, but such a calculation is beyond the scope of this paper.

It is unlikely that any B-type star in BG Gem could be underluminous, compared with a normal main-sequence star. Main-sequence stars accreting material from a disk are at least as luminous as nonaccreting main-sequence stars of the same mass (e.g., Kippenhahn & Meyer-Hofmeister 1977).

The best alternative to this model is a black hole primary. Although less likely than a B-type primary star, a black hole accreting at a small fraction of the Eddington limit might account for the observed radiation at $20\ R_\odot$ (depending on the geometry). To evaluate the plausibility of this model, we considered a disk surrounding a $4.5\ M_\odot$ black hole. The thick, inner disk produces a luminosity of $\sim 10^3\ L_\odot$ if the accretion rate is 1% of the Eddington limit. We naively assumed that the inner disk emits X-rays isotropically; the outer disk absorbs and reradiates this emission at the local blackbody temperature. For a steady-state disk where $H_d \propto R^{-9/8}$, the disk temperature at 4–20 $R_\odot$ is ~ 5000–8000 K. The predicted luminosity of the outer disk in this model, $\sim 100\ L_\odot$, is close to our estimated disk luminosity of 5–10 $L_\odot$ if the inclination is $\sim 85°$.

Our simple example suggests that a black hole accretion disk can plausibly produce the disk emission observed in BG Gem for accretion rates much smaller than the Eddington limit. The model optimistically assumes that the inner disk radiates efficiently, $\sim 10\%$, compared with advection-dominated accretion flows (e.g., Esin, McClintock, & Narayan 1997) and that the outer disk radiates as a blackbody. Despite this optimism, we note that Esin et al. (1997) derive optical luminosities, λF_λ, of $\sim 10^{32}$–10^{33} ergs s^{-1} for quiescent disks and 10^{33}–10^{34} ergs s^{-1} for low-state disks in black hole binaries with inclinations of 60°–90°. The compact disks assumed in the Esin et al. models are more than factor of 100 smaller than the disk in BG Gem, so it

may be possible to achieve the observed optical flux from a larger disk surrounding a black hole in a wider binary system.

The black hole model has one main advantage and one main disadvantage compared with models where the primary is a B-type main sequence star. A black hole accreting at 1% of the Eddington limit easily produces enough high-energy photons to satisfy our constraints on the Hα and Hβ fluxes unless the accretion efficiency is much less than 1% (Esin et al. 1997). But hiding an accreting black hole in an edge-on binary may be more difficult than hiding a B-type main sequence star. The X-ray luminosity, ~ 1300 $L_\odot$, needed to power the observed optical luminosity in BG Gem is roughly 3 orders of magnitude larger than the upper limit derived from the ASM observations, ~ 2 $L_\odot$. The X-ray luminosities of quiescent black hole binary systems are also low, $\lesssim 1$ $L_\odot$ (e.g., McClintock, Horne, & Remillard 1995). However, the region that emits X-rays in a black hole binary is very small, $\sim 10^{10}$–10^{11} cm, and is easily occulted when the binary is viewed at high inclination. For example, Esin et al. (1997) show that the X-ray luminosity of the small disk in an edge-on black hole binary system is several orders of magnitude smaller than the same disk viewed pole-on. We expect that the larger disk in BG Gem can occult a larger fraction of the X-ray flux than an edge-on disk in a smaller binary system. Future calculations of black hole binaries should address this issue.

4. DISCUSSION AND SUMMARY

Our results indicate that BG Gem is a textbook example of a very evolved, semidetached binary system. The system consists of a low-mass, lobe-filling K0 supergiant that transfers material into a disk surrounding a massive primary star. The large, ellipsoidal light variations of the K0 secondary indicate a large mass ratio, $q \approx 0.1$, and large orbital inclination, $i \gtrsim 80°$. The radial velocities of Hα emission in the disk support the large mass ratio. We prefer $i \gtrsim 85°$ to allow the disk to occult the primary star, which is not visible in the optical.

The system is remarkably stable for an interacting binary. There is little scatter in either the optical brightness (for 25 orbital cycles) or the emission-line equivalent widths (for three to four orbital cycles). Studies of archival plate material would place useful constraints on long-term variability and outburst frequency.

Our data are insufficient to choose between the two possible alternatives for the primary star. The optical spectra resemble spectra of several Algol systems—e.g., UU Cancri ($P = 96.7$ days, Eaton, Hall, & Honeycutt 1991) and RZ Ophiuchi ($P = 262$ days, Baldwin 1978; Knee et al. 1986; Zola 1991)—as well as quiescent spectra of several black hole binaries—e.g., V616 Monocerotis ($P = 0.32$ days, McClintock et al. 1995 and references therein) and V404 Cygni ($P = 6.5$ days, Casares et al. 1993 and references therein). None of the long-period Algol binaries have as extreme mass ratios as in BG Gem (see Batten, Fletcher, & MacCarthy 1989), although RZ Oph has $q \approx 0.2$. The structure of the binary in RZ Oph has several other features in common with BG Gem, including a lobe-filling K-type star, an invisible primary, and an extended accretion disk that occults the secondary star at $\phi = 0.5$ (see Olson 1987). However, most of the energy from the disk in RZ Oph is produced by accretion, because the disk in RZ Oph is brighter and less stable than the disk in BG Gem. Produc-

ing a large Hα flux from the intrinsically less luminous disk in BG Gem is also a challenge, as noted above.

BG Gem has many features in common with quiescent black hole binaries, despite the 1–2 order of magnitude difference in orbital periods. Many black hole binaries have ellipsoidal light curves and extreme mass ratios similar to those in BG Gem (e.g., Beekman et al. 1997; Shahbaz et al. 1996; Shahbaz, Naylor, & Charles 1994). Quiescent black hole binaries often have modest emission-line spectra, with strong, double-peaked H I lines and weaker, double-peaked He I lines (e.g., Casares et al. 1993; Filippenko, Matheson, & Ho 1995; McClintock, Horne, & Remillard 1995; Orosz et al. 1998). Higher ionization emission lines, such as He II $\lambda 4686$, appear only in outburst, when the accretion rate through the disk increases dramatically. Quiescent black hole binaries often escape detection as very intense X-ray sources until they undergo major eruptions, and they often remain in quiescence for decades (e.g., Tanaka & Lewin 1995; Ueda et al. 1998). All of the currently known black hole binary systems have small orbital inclinations $i \lesssim 70°$ (see Chen, Shrader, & Livio 1997; Orosz et al. 1998; Filippenko et al. 1999). The $i \gtrsim 85°$ derived here for BG Gem may allow the disk to occult even an intense X-ray source (see Sobczak et al. 1999a, 1999b, and references therein for typical outburst fluxes). Despite the lack of X-rays, BG Gem may still contain a black hole primary surrounded by a quiescent accretion disk.

If confirmed, BG Gem would be the black hole binary with the longest known orbital period. Other black hole binaries have periods of a few days or less. Any black hole binary is a challenge to modern theories of the evolution of binary systems (e.g., Kalogera 1999). BG Gem would provide a severe test of these theories. BG Gem would also be the only eclipsing system known among black hole binaries. The black hole mass is unambiguous in an eclipsing binary. Our limit for the primary mass is close to the maximum possible neutron star mass (see, for example, Burrows 1998). BG Gem thus may place new constraints on the minimum black hole mass.

With these considerations in mind, it is clear that additional observations are needed to understand the nature of the primary in BG Gem. Ultraviolet spectra at 1000–3000 Å would probe the continuum and emission lines produced in the inner portions of the accretion disk and might reveal stellar absorption lines if the primary is a B-type star. Better limits on the X-ray flux from instruments on board *Chandra* and the *XMM* would also provide better constraints on the nature of the primary. Detection of an X-ray source that is eclipsed at primary minima would favor a black hole primary, because B-type main sequence stars are weak X-ray sources.

Whatever the nature of the primary, future studies of the secondary star and the accretion disk surrounding the primary should yield a better understanding of accretion in wide binary systems. Eclipses of the blue continuum and the emission lines provide useful information about disk structure, through maximum entropy reconstruction, among other techniques. Higher resolution observations of Mg I and other absorption features probe conditions in the secondary star as well as the cool, outer portions of the disk. Near-infrared observations covering the orbit would improve mass estimates for the secondary star derived from ellipsoidal variations and might reveal emission from an optically thick "bright spot," where material lost by the K0

supergiant impacts the disk. Emission from an optically thin spot might be visible in Hα or Hβ. Finally, high-resolution observations might yield a radial velocity curve for the primary and improved estimates for the mass ratio. The small distance and reddening make BG Gem a prime target for these and other observations of a binary system at an interesting phase of its evolution.

REFERENCES

Baldwin, B. W. 1978, ApJ, 226, 937
Barnes, J. V., & Hayes, D. S. 1982, IRS Standard Star Manual (Tucson: NOAO)
Batten, A. H., Fletcher, J. M., & MacCarthy, D. G. 1989, Publ. Dom. Astrophys. Obs. Victoria, 17, 1
Beekman, G., Shahbaz, T., Naylor, T., Charles, P. A., Wagner, R. M., & Martini, P. 1997, MNRAS, 290, 303
Bessell, M. S. 1990, PASP, 102, 1181
Bessel, M. S., & Brett, J. M. 1988, PASP, 100, 1134
Burrows, A. 1998, in Ringberg Workshop on Nuclear Astrophysics, ed. E. Müller & W. Hillebrandt (Garching bei München: Max-Planck-Institut für Astrophysik), 76
Casares, J., Charles, P. A., Naylor, T., & Pavlenko, E. P. 1993, MNRAS, 265, 834
Chen, W., Shrader, C. R., & Livio, M. 1997, ApJ, 491, 312
Eaton, J. A., Hall, D. S., & Honeycutt, R. K. 1991, ApJ, 376, 289
Esin, A. A., McClintock, J. E., & Narayan, R. 1997, ApJ, 489, 865
Fabricant, D. G., Cheimets, P., Caldwell, N., & Geary, J. 1998, PASP, 110, 79
Filippenko, A., Leonard, D. C., Matheson, T., Li, W., Moran, E. C., & Riess, A. G. 1999, PASP, in press
Filippenko, A., Matheson, T., & Ho, L. C. 1995, ApJ, 455, 614
Hakkila, J., Myers, J., Stidham, B., & Hartmann, D. 1997, AJ, 114, 2043
Hoffmeister, C. 1933, Sonn. Mitt No. 22
Jacoby, G., Hunter, D. A., & Christian, S. 1984, ApJS, 56, 257
Jensch, A. 1938, KVBB, No. 19
Kalogera, V. 1999, ApJ, 521, 723
Kenyon, S. J., & Garcia, M. R. 1986, AJ, 91, 125
Kenyon, S. J., & Hartmann, L. W. 1987, ApJ, 323, 714
Kenyon, S. J., Oliversen, N. G., Mikołajewska, J., Mikołajewski, M., Stencel, R. E., Garcia, M. R., & Anderson, C. M. 1991, AJ, 101, 637
Kenyon, S. J., & Webbink, R. F. 1984, ApJ, 279, 252
Kholopov, P. N., ed. 1985, General Catalog of Variable Stars (4th ed; Moscow: Nauka)
Kippenhahn, R., & Meyer-Hofmeister, E. 1977, A&A, 54, 539
Knee, L. B. G., Scarfe, C. D., Mayor, M., Baldwin, B. W., & Meatheringham, S. J. 1986, A&A, 168, 72
Kurtz, M. J., & Mink, D. J. 1998, PASP, 110, 934
Levine, A. M., Bradt, H., Cui, W., Jernigan, J. G., Morgan, E. H., Remillard, R., Shirey, R. E., & Smith, D. A. 1996, ApJ, 469, 33
Lucy, L. B., & Sweeney, M. A. 1971, AJ, 76, 544
Mathis, J. S. 1990, ARA&A, 28, 37
McClintock, J. E., Horne, K., & Remillard, R. A. 1995, ApJ, 442, 358
Monet, D. G. 1979, ApJ, 234, 275
Neckel, T., & Klare, G. 1980, A&AS, 42, 251
O'Connell, R. W. 1973, AJ, 78, 1074
Olson, E. C. 1987, AJ, 94, 1309
———. 1991, AJ, 102, 1423
Orosz, J. A., Jain, R. K., Bailyn, C., McClintock, J. E., & Remillard, R. A. 1998, ApJ, 499, 375
Rieke, G. H., & Lebofsky, M. J. 1985, ApJ, 288, 618
Shahbaz, T., Naylor, T., & Charles, P. A. 1994, MNRAS, 268, 756
Shahbaz, T., van der Hooft, F., Charles, P. A., Casares, J., and van Paradijs, J. 1996, MNRAS, 282, L47
Sobczak, G., McClintock, J. E., Remillard, R. E., Bailyn, C. D., & Orosz, J. A. 1999a, ApJ, 520, 776
Sobczak, G., McClintock, J. E., Remillard, R. E., Levine, A. M., Morgan, E. H., Bailyn, C. D., & Orosz, J. A. 1999b, ApJ, 517, L121
Tanaka, Y., & Lewin, W. H. G. 1995, in X-ray Binaries, edited by W. H. G. Lewin, J. van Paradijs, & E. P. J. van den Heuvel (Cambridge: Cambridge Univ. Press), 126
Tonry, J., & Davis, M. 1979, AJ, 84, 1511
Ueda, Y., Ishida, M., Inoue, H., Dotani, T., Greiner, J., & Lewin, W. H. G. 1998, ApJ, 508, L167
Vrielmann, S., Horne, K., & Hessman, F. V. 1999, MNRAS, 306, 766
Wilson, R. E. 1990, ApJ, 356, 613
———. 1994, PASP, 106, 921
Wilson, R. E., & Devinney, E. J. 1971, ApJ, 166, 605
Worthey, G. 1994, ApJS, 95, 107
Zola, A. 1991, Acta Astron., 41, 213